

Electronic Supporting Information

A Freestanding 3D Heterophase Tungsten Disulfide-based Aerogel as an ultrathin microwave absorber in Ku-band

Jun Zhou, Jialiang Luo, Gazi Hao, Fan Guo, Guigao Liu, Hu Guo, Guangpu

Zhang, Lei Xiao, Yubing Hu*, Wei Jiang*

National Special Superfine Powder Engineering Technology Research Center,

Nanjing University of Science and Technology, Nanjing 210094, Jiangsu, China

*Corresponding author: hyb@njust.edu.cn (Yubing Hu) and climentjw@126.com

(Wei Jiang)

Experimental

Synthesis of 1T-WS₂/CNT/rGO

Typically, 40 mg of cetyltrimethylammonium bromide (CTAB) were added to 40 mL of N,N-Dimethylformamide (DMF) solution and stirred for 10 min. Secondly, 40 mg of GO and 10 mg of carboxylated CNTs were sequentially added to the above solution for 30 min of sonication and 30 min of stirring, respectively. Thirdly, 200 mg of ammonium tetrathiotungstate were added to the above solution by sonication for 30 min and stirring for 30 min, respectively. Fourthly, the mixed solution were transferred to a 100 mL Teflon-lined stainless steel autoclave, and kept in oven at 200 °C for 10 h. Fifthly, the product were collected after cooling to room temperature and washed three times with DMF and deionized water to remove residues. Sixthly, the washed product were added to 5 mL of deionized ultrasonic for 10 min, and placed in a low temperature box with -65° C. for 6h. Finally, the product were freeze-dried for 48 h to collect the final product, labeled as 1T-WS₂/CNT/rGO (GCW-1T). For comparison, the product 2H-WS₂/CNT-rGO (GCW-2H) were obtained by annealing GCW-1T under NH₃ atmosphere at 550 °C for 2 h. Besides, 1T-WS₂/CNT (CW-1T) and 2H-WS₂/CNT (CW-2H) were obtained through the same procedure without GO.

Characterization

The phase of the sample was analyzed by XRD (Bruker D8 Advance, Germany) at 5-80°. Raman spectra were obtained using a Raman spectrometer (LabRAM HR Evolution, HORIBA JobinYvon, France) at room temperature using the 532 nm line as the excitation source. XPS measurements were carried out on an ESCALAB 250Xi

spectrometer (Thermo Scientific, USA) equipped with a pass energy of 30 eV with a power of 100 W (10 kV and 10 mA). The microstructure was observed and analyzed by FESEM (ZEISS Gemini SEM 300, Germany), TEM and HRTEM (FEI Talos F200s, American). HAADF-STEM images were captured with a FEI Super-X TEM equipped with a cold field-emission gun. The adsorption-desorption isotherm is obtained by the specific surface area analyzer (Micromeritics ASAP 2460, USA). Wettability behaviors were observed using a contact angle meter (CAM, Kono, C20).

Electromagnetic parameters

The absorption parameters of the sample were obtained by the network analyzer (AV3672B-S, China) at the frequency (2-18 GHz). The sample preparation is divided into three steps. First, evenly mix the sample with molten paraffin. To obtain the samples for microwave measurement, the powders were uniformly mixed with molten paraffin in proportions (samples filling ratios of 35%, 30%, 25% and 20%, respectively). Then, natural curing. Finally, the mixtures were pressed into a cylindrical shape with a mold, with an inner diameter of 3.04 mm, an outer diameter of 7 mm and thicknesses of 2-3 mm.

The microwave absorption performance of absorbers were evaluated by the reflection loss (RL), which could be calculated by the following equations according to the transmission line theory:^{1,2}

$$RL(\text{dB}) = 20 \lg \left| \frac{Z_{in} - Z_0}{Z_{in} + Z_0} \right| \quad (\text{S1})$$

$$Z_{in} = Z_0 (\mu_r / \epsilon_r)^{1/2} \tanh \left[j (2\pi f d / c) (\mu_r \epsilon_r)^{1/2} \right] \quad (\text{S2})$$

where Z_{in} is the input impedance of a single layer of absorbing material, Z_0 is the free space impedance, ϵ_r is the complex permittivity, μ_r is the complex permeability, f is the test frequency and d is the thickness of the absorbing material.

The classical Debye theory was used to analyze the dielectric loss, and can be described in following equation:^{3,4}

$$\epsilon' = \epsilon_\infty + \frac{\epsilon_s - \epsilon_\infty}{1 + \omega^2 \tau^2} \quad (S3)$$

$$\epsilon'' = \frac{\epsilon_s - \epsilon_\infty}{1 + \omega^2 \tau^2} \omega \tau + \frac{\sigma}{\omega \epsilon_0} \quad (S4)$$

$$\left(\epsilon' - \frac{\epsilon_s + \epsilon_\infty}{2} \right)^2 + (\epsilon'')^2 = \left(\frac{\epsilon_s - \epsilon_\infty}{2} \right)^2 \quad (S5)$$

where ϵ_s is the stationary dielectric constant, ϵ_∞ represents the optical dielectric constant, ω is the angular frequency, τ is the relaxation time and σ is the electrical conductivity.

The attenuation ability of microwave absorber be explained by attenuation constant (α), which can be described as:⁵

$$\alpha = \frac{\sqrt{2\pi f}}{c} \times \sqrt{(\mu''\epsilon'' - \mu'\epsilon') + \sqrt{(\mu''\epsilon'' - \mu'\epsilon')^2 + (\mu'\epsilon'' + \mu''\epsilon')^2}} \quad (S6)$$

where c is the velocity of light in free space.

According to Maxwell-Garnett theory:⁶

$$\frac{MG}{\epsilon_{eff}} = \epsilon_1 \frac{(\epsilon_2 + 2\epsilon_1) + 2f_v(\epsilon_2 - \epsilon_1)}{(\epsilon_2 + 2\epsilon_1) - f_v(\epsilon_2 - \epsilon_1)} \quad (S7)$$

where $\frac{MG}{\epsilon_{eff}}$ is the effective permittivity of material, (ϵ_1) is the solid permittivity and (ϵ_2) is void permittivity.

It is hypothesized that the absorber (t_m) and the corresponding absorption

frequency (f_m) satisfy the following conditions:⁷

$$t_m = \frac{n\lambda}{4} = \frac{nc}{4f_m \sqrt{|\mu_r \epsilon_r|}} \quad (n = 1, 3, 5 \dots) \quad (S8)$$

The impedance matching is an important indicator of electromagnetic wave absorption, and can be expressed as follows:⁸

$$Z = |Z_{in} / Z_0| = (\mu_r / \epsilon_r)^{1/2} \tanh \left[j(2\pi f d / c)(\mu_r \epsilon_r)^{1/2} \right] \quad (S9)$$

RCS Simulation

To verify the actual radar cross section (RCS) of the GCW-1T, High Frequency Structure Simulator (HFSS 15.0) was used to simulate the RCS of absorber. According to the widely accepted metal substrate model, the plate is defined as a perfect conductor with a size of 180*180*5mm. Specifically, the thickness of the absorber above the metal substrate is set to be 1.15mm, and length for each side are set as 180 mm. The model is placed on the X-Y-Z plane, defining the excitation mode of the plane wave, with normal incidence from the Z axis. The plane wave incidence direction is determined by theta and phi in spherical coordinates. Herein, the incident directions of two plain waves are described as (theta=0°, phi=0°) and (theta=45°, phi=0°), respectively. Besides, the operating frequency is determined as 15.44 GHz corresponding to the optimal absorption properties. The boundary conditions are set to Radiation Boundaries. Typically, the metal substrate RCS calculation equation can be expressed as:⁹⁻¹¹

$$\sigma = \frac{4\pi A^2}{\gamma^2} \times \cos^2 \theta \times \frac{\sin^2 f_1}{f_1} \times \frac{\sin^2 f_2}{f_2} \quad (S10)$$

where σ is the RCS, A is the area of the plate (for a typical metal substrate, $A = ab$, a and b is the side of the plate, respectively), θ is the angle of incident waves, φ is the angle between incident waves and a , λ is the wavelength. $f_1 = k \times a \times \sin\theta \times \cos\varphi$, $f_2 = k \times b \times \sin\theta \times \cos\varphi$, k is the wave number, $k = 2\pi/\lambda$.

Results and discussion



Fig. S1. 1T-WS₂/CNT/rGO Aerogel.

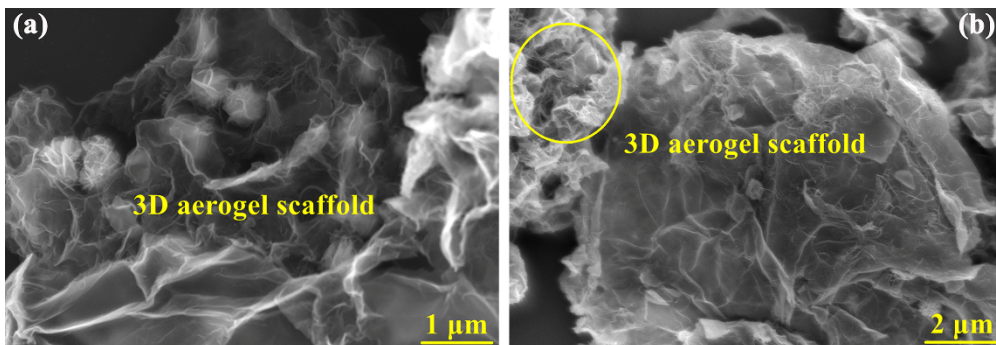


Fig. S2. FESEM images of samples: (a) GCW-1T and (b) GCW-2H.

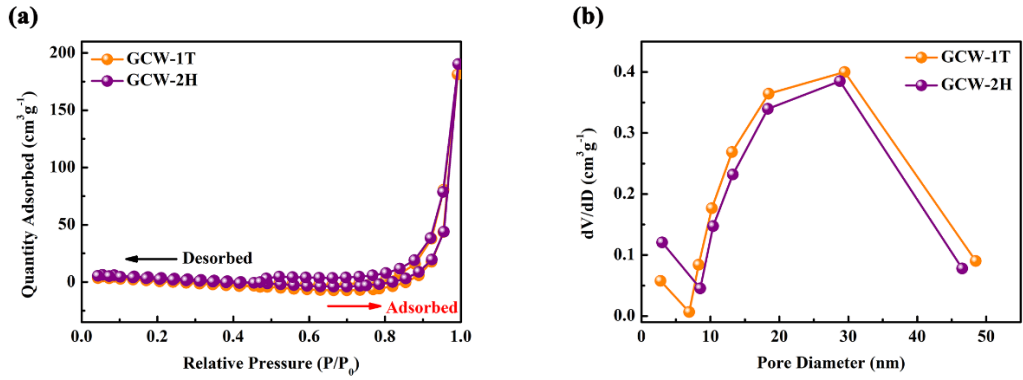


Fig. S3. (a) N_2 adsorption-desorption isotherms and (b) pore size distribution of the samples.

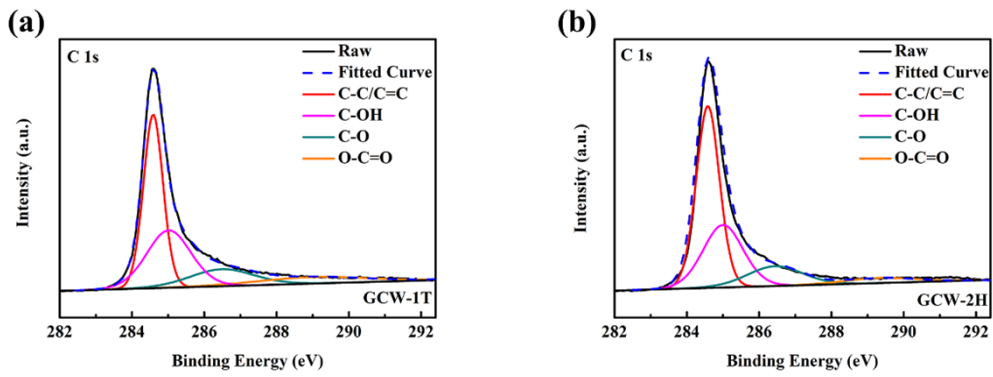


Fig. S4. XPS spectra with C 1s of samples: (a) GCW-1T and (b) GCW-2H.

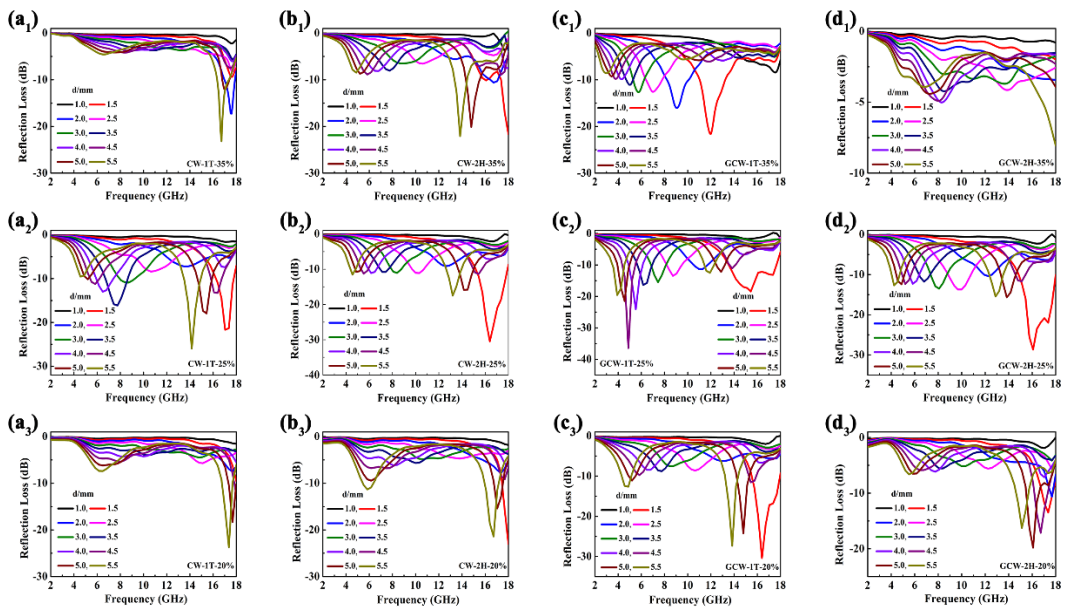


Fig. S5. Reflection loss curves of the samples with different thicknesses and filling ratio: (a) CW-1T, (b) CW-2H, (c) GCW-1T and (d) GCW-2H.

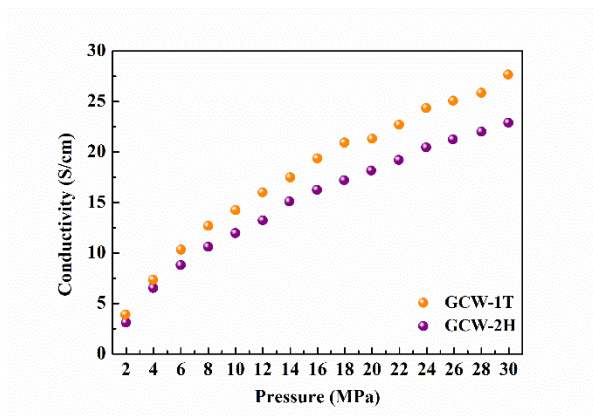


Fig. S6. Electrical conductivity curves of samples with different pressure.

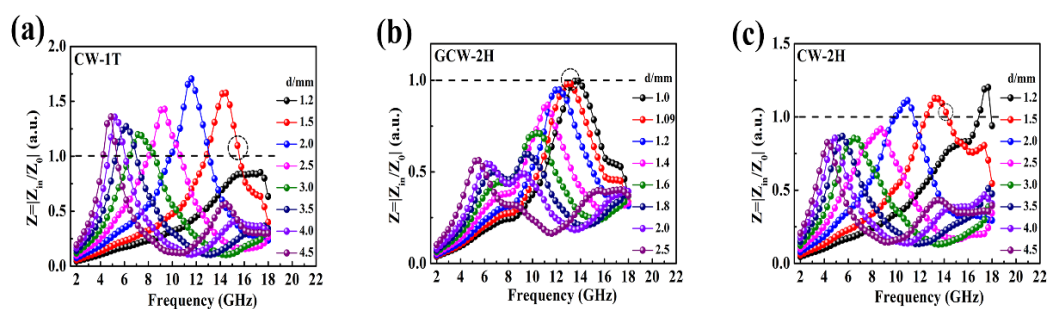


Fig. S7. Dependence on frequency of the impedance matching for the sample: (a) CW-1T, (b) GCW-2H and (c) CW-1T.

Table S1 Comparison of microwave absorption properties of the carbon-based materials.

Samples	EMA performances			Ref
	Matching thickness (mm)	Optimal RL Value (dB)	EAB (GHz)	
MXene-CNT	3.95	-40.00	4.20	[12]
rGO/Ni	2.00	-39.03	4.30	[13]
N-graphene foam	3.50	-53.90	4.56	[14]
CoFe@C	2.40	-31.00	4.08	[15]
NiFe/C	3.00	-52.99	1.81	[16]

MXene/CoNi/N-CNT	3.8	-52.64	3.12	[17]
CAF-rGO/epoxy	2.20	-35.70	3.55	[18]
GO/Bi-MOF/C	3.70	-33.80	3.40	[19]
CoNC/Carbon Fibers	2.90	-45.50	1.00	[20]
SiO ₂ /C	1.50	-43.00	3.68	[21]
Graphene/CIP/PMMA	2.10	-54.40	3.41	[22]
MXene/Ni/N-CNT	1.49	-57.78	3.44	[23]
CoS ₂ /Cu ₂ S/N,S-C	4.50	-51.68	3.84	[24]
CNFs-SiCN	1.85	-36.30	3.00	[25]
GCW-1T	1.15	-56.63	3.84	This work

References

1. X. Yuan, R. Wang, W. Huang, Y. Liu, L. Zhang, L. Kong and S. Guo, *Chem. Eng. J.*, 2019, **378**, 122203.
2. Y. Liu, Z. Chen, Y. Zhang, R. Feng, X. Chen, C. Xiong and L. Dong, *ACS Appl. Mater. Interfaces*, 2018, **10**, 13860-13868.
3. P. Liu, S. Gao, W. Huang, J. Ren, D. Yu and Y. He, *Carbon*, 2020, **159**, 83.
4. W. Liu, S. Tan, Z. Yang and G. Ji, *Carbon*, 2018, **138**, 143-153.
5. P. Wang, L. Cheng and L. Zhang, *Carbon*, 2017, **125**, 207-220.
6. B. Quan, X. Liang, G. Ji, Y. Zhang, G. Xu and Y. Du, *ACS Appl. Mater. Interfaces*, 2017, **9**, 38814-38823.
7. N. Li, R. Shu, J. Zhang and Y. Wu, *J. Colloid. Interface. Sci.*, 2021, **596**, 364.

8. T. Liu, X. Xie, Y. Pang and S. Kobayashi, *J. Mater. Chem. C*, 2016, **4**, 1727-1735.
9. L. Huang, J. Li, Z. Wang, Y. Li, X. He and Y. Yuan, *Carbon*, 2019, **143**, 507-516.
10. N.N. Youssef, *Proc. IEEE.*, 1989, **77**, 722-734.
11. R. Ross, *IEEE Trans. Antenn. Propag.*, 1966, **14**, 329-335.
12. X. Liu, N. Chai, Z. Yu, H. Xu, X. Li, J. Liu, X. Yin and R. Riedel, *J. Mater. Sci. Technol.*, 2019, **35**, 2859-2867.
13. W. Xu, G. Wang and P. Yin, *Carbon*, 2018, **139**, 759-767.
14. P. Liu, Y. Zhang, J. Yan, Y. Huang, L. Xia and Z. Guang, *Chem. Eng. J.*, 2019, **368**, 285-298.
15. S. Wei, T. Chen, Q. Wang, Z. Shi, W. Li and S. Chen, *J. Colloid Interface. Sci.*, 2021, **593**, 370-379.
16. L. Weng, X. Lei, J. Liu, H. Hu, J. Wang and Z. Zhang, *J. Alloys. Compd.*, 2022, **906**, 164301.
17. J. Zhou, F. Guo, J. Luo, G. Hao, G. Liu, Y. Hu, G. Zhang, H. Guo, H. Zhou and Wei Jiang, *J. Mater. Chem. C*, 2022, **10**, 1470-1478.
18. S. K. Singh, Y. K. Penke, J. Ramkumar, M.J. Akhtar and K. K. Kar, *J. Alloys. Compd.*, 2022, **901**, 163659.
19. X. Fan, A. Zhang, M. Li, H. Xu, J. Xue, F. Ye and L. Cheng, *J. Mater. Sci. Mater. Electron*, 2020, **31**, 11774-11783.
20. T. Wu, X. Huan, X. Jia, G. Sui, L. Wu, Q. Cai and X. Yang, *Composites Part B.*, 2022, **233**, 109658.
21. Q. Li, J. Zhu, S. Wang, F. Huang, Q. Liu and X. Kong, *Carbon*, 2020, **161**, 639-

646.

22. Y. Zuo, Z. Yao, H. Lin, J. Zhou, J. Lu and J. Ding, *Composites Part B.*, 2019, **179**, 107533.

23. J. Zhou, G. Zhang, J. Luo, Y. Hu, G. Hao, H. Guo, F. Guo, S. Wang and W. Jiang, *Chem. Eng. J.*, 2021, **426**, 130725.

24. Y. Li, L. Gai, G. Song, Q. An, Z. Xiao and S. Zhai, *Carbon*, 2022, **186**, 238-252.

25. X. Liu, M. Li, H. Liu, W. Duan, C. Fasel, Y. Chen, F. Qu, W. Xie, X. Fan, R. Riedel and A. Weidenkaff, *Carbon*, 2022, **188**, 349-359.